JCTC Journal of Chemical Theory and Computation

Article

pubs.acs.org/JCTC

Theoretical Determination of Electronic Spectra and Intersystem Spin−Orbit Coupling: The Case of Isoindole-BODIPY Dyes

Marta E. Alberto,* Bruna C. De Simone,* Gloria Mazzone, Angelo D. Quartarolo, and Nino Russo

Dipartimento di Chimica e Tecnologie Chimiche, Università della Calabria, I-87036 Arcavacata di Rende, Italy

Supporting Information

ABSTRACT: Density functional theory and its time-dependent extension (DFT, TDDFT) has been herein employed to elucidate the structural and electronic properties for a series of isoindole-boron dipyrromethene (isoindole-BODIPY) derivatives. The role played by both the nature and the positions of the substituents on intersystem spin-crossing has been investigated computing the spin−orbit matrix elements between singlet and triplet excited state wave functions weighted by the TDDFT transition coefficients. Their potential therapeutic use as photosensitizers in photodynamic therapy (PDT) is proposed on the basis of their strong absorbance in the red part of the visible spectrum, vertical triplet energies resulting higher than 0.98 eV, and the spin−orbit matrix elements that result to be comparable with different drugs already used in PDT.

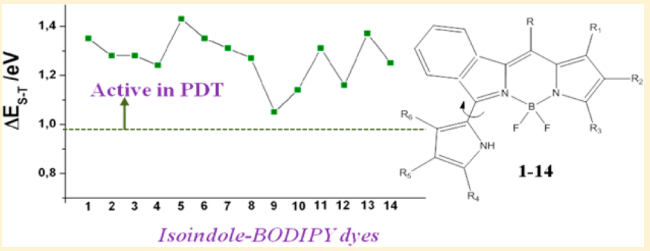

1. INTRODUCTION

The 4,4-difluoro-4-bora-3*a*,4*a*-diaza-*s*-indacene (BODIPY) and its aza (aza-BODIPY) derivatives have attracted great attention due to their photophysical and thermodynamic properties. Actually, these compounds show large absorption extinction coefficients, sharp emissions, and quantum fluorescence yields as well as high redox and thermodynamic stability and relative simple synthesis.[1−3] Starting from the first synthesized aza-BODIPY in 1943[4] and BODIPY in 1960[5] proposed as colorants, many different new molecules containing the aza-BODIPY and BODIPY cores have been proposed for a huge number of applications ranging from biological labeling, electroluminescent devices, tunable laser dyes, solid-state solar concentrators, fluorescent switches, and fluorophores in sensors.[3] More recently, the seminal works of O'Shea and co-workers in 2002 and of other groups[6,7] have demonstrated that these compounds can be used as efficient photosensitizers in photodynamic therapy (PDT).[8,9] This emerging noninvasive medical therapy is nowadays used for the treatment of different kinds of tumors (e.g., esophagus, bladder, early lung, breast, and prostate cancers), age-related macular degeneration, and skin diseases,[10−15] and its clinical efficiency is currently explored for other diseases, such as infections, cardiovascular, and wound healing.[16−18] The working mechanism of PDT requires a combination of a light source, a photosensitizer drug dose, and the presence in human tissues of molecular oxygen $^3O_2$ ($^3\Sigma_g^-$). The light is provided by a laser operating at a given frequency, the $^3O_2$ is naturally present in the human tissue, and the photosensitizer (PS) can be injected in the body. The in locu generated cytotoxic oxygen species induces apoptosis and/or necrosis of target cells. The mechanism of generation of singlet oxygen $^1O_2$ ($a^1\Delta_g$) as the key cytotoxic agent, (usually referred to as Type II PDT mechanism) mainly proceeds throughout following three photochemical steps:[8,9,19] (i) the PS is excited from the ground state S_0 to the first excited S_1 one by illumination using light of a specific intensity and wavelength; (ii) the PS S_1 state decays to the first triplet excited state (T_1) through a radiationless intersystem spin-crossing process (ISC); and (iii) the energy coming by the previous process is transferred to molecular oxygen, and if the amount of transferred energy is higher than 0.98 eV,[20] the highly reactive species $^1O_2$ is formed ($^3\Sigma_g^- \rightarrow {}^1\Delta_g$ electronic transition). As a consequence, an efficient PDT photosensitizer must mainly possess a red-shifted electronic absorption band that falls in the so-called therapeutic window (650−800 nm) to penetrate human tissues, allowing the treatment of deeper tumors, a high intersystem spin-crossing probability, an exited state with different spin multiplicity with respect to that in the ground state with an energy greater than 0.98 eV, and, consequently, good singlet oxygen quantum yield (Φ_Δ). Other requested properties include solubility in aqueous media, redox stability, absence of intermolecular aggregation phenomena, which decreases the photodynamic action, and no toxicity in the dark. Many photosensitizers approved for clinical use belong to the porphyrin-like class of molecules (photophrin,[21] a mixture of hematoporphyrin monomers, dimers, and oligomers, *m*-tetrahydroxyphenylchlorin, Foscan,[22] lutetium texaphyrin, Lutrin[23]). However, also, the synthesis of a new nonporphyrin potential PDT drug represents an important growing research field.[6,24−27] In this paper, we will present a theoretical study of the structures and photophysical properties of a series of

Received: May 16, 2014

dx.doi.org/10.1021/ct500426h | *J. Chem. Theory Comput.* XXXX, XXX, XXX−XXX

Scheme 1. Chemical Structures of BODIPY Dyes Investigated in This Work

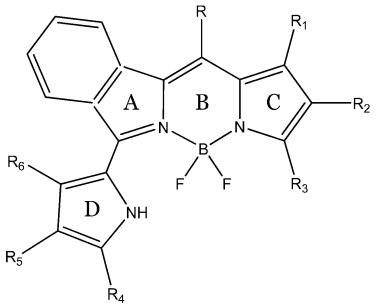

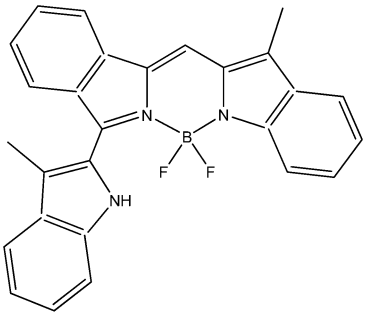

14

1: R,R1,R2,R3,R4,R5,R6 = H
2: R3,R4=-CH_3 ; R,R1,R2,R5,R6=H
3: R1,R3,R4,R6=-CH_3 ; R,R2,R5=H
4: R1,R3,R4,R6=-CH_3 ; R=H; R2,R5=-CH_2CH_3
5: R=-CH_3 ; R1,R2,R3,R4,R5,R6=H
6: R,R1,R3,R4,R6=-CH_3 ; R2,R5= H
7: R,R1,R3,R4,R6 =-CH_3 ; R2,R5= -CH_2CH_3
8: R1,R3=-CH_3 ; R,R2,R4,R5,R6=H
9: R1,R4,R6=-CH_3 ; R,R2,R5=H ; R3= Ar
10: R,R1,R4,R6=-CH_3 ; R2,R5= -CH_2CH_3; R3= Ar
11: R1,R3,R4,R6=-CH_3 ; R2,R5=H ; R= Ar
12: R1,R4,R6=-CH_3 ; R2,R5=H ; R,R3=Ar
13: R1,R2,R3,R4,R5,R6=H ; R=Ar

Ar =

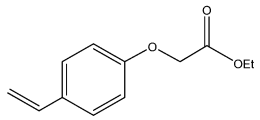

Table 1. Selected Geometrical Parameters and λ_{max} for Molecule 3, Calculated by Using Different XC Functionals and Compared with Experimental Results[28a]

	B−N1	B−N2	B−N3	B−F1	B−F2	F1−N3	F2−N3	F2−H1	F2−B−N1	F2−B−N2	φ1	λ (nm)
wB97XD	1.534	1.574	3.093	1.390	1.425	3.015	2.760	1.880	109.5	107.9	−37.6	516
PBEO	1.537	1.571	3.072	1.386	1.422	2.999	2.742	1.845	109.2	108.3	−34.0	543
B3LYP	1.542	1.577	3.102	1.393	1.429	3.040	2.761	1.868	109.2	108.3	−35.8	547
M06	1.539	1.579	3.073	1.380	1.413	2.983	2.765	1.873	109.4	108.3	−34.2	551
M062X	1.538	1.578	3.067	1.383	1.414	2.958	2.770	1.892	109.6	108.1	−36.3	529
exptl	1.527	1.563	3.109	1.379	1.411	3.014	2.792		109.7	108.2	−37.3	609

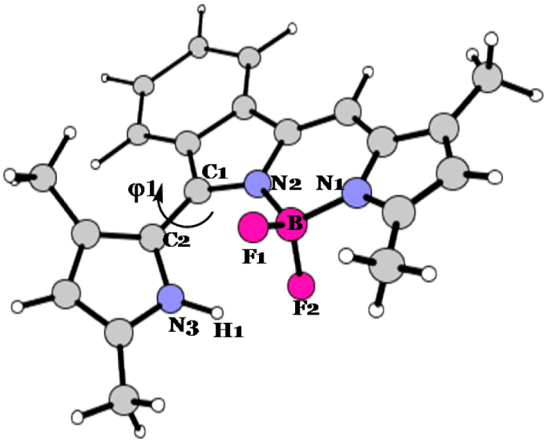

[a]Distances are in Å and angles in degrees.

isoindole-BODIPY dyes recently synthesized and characterized by using X-ray analysis and UV−vis spectroscopy[28] (Scheme 1, structures **1**−**6**). From our results emerge that these compounds could be good candidates for their use in photodynamic therapy as well as in biological imaging. Previous papers have largely demonstrated that theoretical computations based on first-principles methods can reliably predict or reproduce and rationalize electronic transitions and singlet−triplet energy gaps.[29−41] Furthermore, the computational approach is able to give insights about the ISC mechanism[29,30,33,34] since it is known, from the application of perturbation theory to radiationless transitions (e.g., $S_1 \rightarrow T_1$), that the transition probability (k_{ISC}) depends quadratically on the corresponding matrix element of the spin−orbit quantum operator, H_{so}.

dx.doi.org/10.1021/ct500426h | J. Chem. Theory Comput. XXXX, XXX, XXX−XXX

2. COMPUTATIONAL DETAILS

All the computations presented in this work have been carried out by using the Gaussian 09[42] code at DFT and its time-dependent formulation TDDFT[43] levels of theory.

A preliminary benchmark study has been performed on one of the molecules (namely, **3**) testing different exchange-correlation (XC) functionals in order to select the most appropriate one to describe the other investigated systems. In particular, ground state molecular optimizations have been performed in solvent by using M06, M062X,[44] ωB97XD,[45,46] and PBE0[47,48] XC functionals, and their performances have been evaluated comparing both calculated geometrical parameters and absorption electronic spectra with available experimental data.

Solvent effects have been included by means of the polarizable continuum model (PCM),[49,50] taking into account the dielectric media of dichloromethane (ε = 8.93).

The M06 exchange-correlation functional has been adopted as the most suitable and has been used in conjunction with 6-31+G* basis sets for all the succeeding geometry optimizations and to reproduce the electronic spectra in two different environments (dichloromethane (ε = 8.93) and water (ε = 79.3)).

Spin−orbit matrix elements have been computed by using the DALTON code[51] testing, for molecule **1**, both the Breit−Pauli method[51] and atomic mean field approximation.[52] Both the employed levels of theory provide very similar values (vide infra); consequently, for all the other considered compounds, the spin−orbit matrix elements have been computed by using only the atomic mean field approximation that requires low computational costs as also previously observed.[29,30]

Because of the presence of only a few hybrid functionals available in DALTON to perform these calculations, B3LYP[52,53] has been selected and used on the previously M06 optimized geometries.

This choice was further driven by the previous successful use of B3LYP[29] to calculate the spin−orbit matrix elements for the active PDT compound selected for the comparison.

The density difference plots between the excited and ground state total electronic densities have been obtained throughout the computation of the *Z*-vector available from the computation of TD-DFT forces.[54]

3. RESULT AND DISCUSSION

3.1. Benchmark of XC Functionals and Ground State Properties. In order to select the most appropriate XC functional to accurately describe both geometrical parameters and electronic transition energies for the systems under evaluation, a series of preliminary computations have been carried out testing different XC density functionals against the experimental data available for molecule **3**.

Results, collected in Table 1, indicate that all the employed XC functionals are able to reproduce with accuracy the geometrical parameters. Nevertheless, M06 has proven to be better also in predicting the maximum absorption peak in the Q-band. Actually, the experimental value has been provided with a difference of only 58 nm (about 0.1 eV) shifted in the blue part of the UV−vis spectrum. As a consequence, M06 has been chosen as the most suitable XC functional for the description of all the other considered systems. This result also agrees with other previous benchmarks.[37,39]

From a structural point of view, all the studied systems consist of a central BODIPY unit embedded with different substituents. Compounds **1**−**8** and **14** show rigid structures with conformational flexibility around the φ_1 torsional angle (Scheme 1). On the contrary, the presence of a large Ar substituent increases the conformational degree of freedom for compounds **9**−**13**. For all the compounds, we find a reasonable agreement with the main geometrical parameters determined by X-ray analysis[28] (see Table S1 in the Supporting Information). The main torsional angles are reported in Table 2 and compared with the corresponding experimental values. On the basis of the obtained structures, it is possible to establish that the values of the φ_1 angle in the different compounds are due to a delicate balance between steric hindrance (e.g., the hydrogen and methyl groups on the adjacent rings), conjugation effects, and hydrogen bond formation with the BF_2 group. In particular, we note that, in the compounds in which the substituent R6 is a H atom (**1**, **2**, **5**, **8**, **13**), the φ_1 angle assumes values of about 20°, whereas the presence in this position of a CH_3 group (**3**, **4**, **14**, **6**, **7**, **9**−**12**) increases the torsional angle values by about 10° due the higher steric hindrance between H and CH_3 interactions (see Table

Table 2. Selected Bond Lengths [Å] and Angles [deg] for BODIPYs, Calculated at M06/6-31+G* Level[a]

	H1−F2	N1−F2	φ1	φ2	φ3
1	1.831	2.734	−22.2		
2	1.837	2.740	−22.1		
3	1.872	2.765	−34.2		
		(2.765)	*(−37.3)*		
4	1.872	2.763	−35.2		
5	1.842	2.735	26.0		
		(2.773)	*(28.3)*		
6	1.868	2.751	−36.7		
7	1.889	2.772	−36.9		
8	1.843	2.743	−23.5		
		(2.778)	*(−28.6)*		
9	1.862	2.740	−35.8	−6.2	
10	1.903	2.780	−37.6	16.3	
11	1.890	2.764	−36.7		125.8
		(2.864)	*(−39.6)*		
12	1.855	2.750	−35.5	172.1	127.8
13	1.846	2.746	−26.2		132.4
14	1.882	2.773	−38.4		

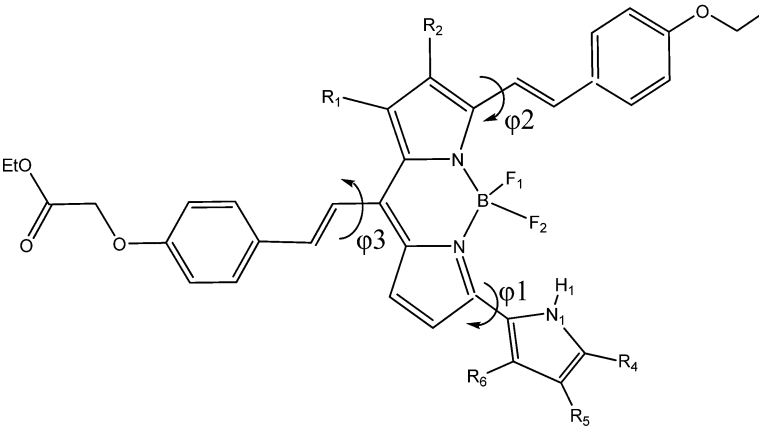

[a]Available experimental values are reported in parentheses.[28]

dx.doi.org/10.1021/ct500426h | J. Chem. Theory Comput. XXXX, XXX, XXX−XXX

2). For compounds **9**−**13**, which contain one or two large Ar groups, the conformational flexibility increases due to the presence of other torsional angles (the main angles are φ_2 and φ_3). In compound **9**, in which the Ar is linked in position R_3, the φ_2 assumes a value of 6.2° (see Table 2), whereas, in **10**, the value becomes 16.3° due the presence of a CH_3 in position R_2. The same difference of about 10° is observed going from compound **11** to **13**, in which, besides the Ar lying in position R, a methyl group occupies the position R1. Finally, in **12**, the presence of two Ar in positions R and R3 gives rise to a structure with a φ_2 angle close to the planarity value (172.2°) and a φ_1 that assumes a high value (132.4°). As in **11** and **13**, also in **12**, the φ_3 value strongly deviates from the planarity since, in the R position, the delocalization of cycle B is poor.

3.2. Electronic Excitations. The maximum absorption peaks in the Q-band region computed for all the investigated systems are reported in Table 3 and compared with the available experimental λ_{max} values.[28]

Table 3. Main Vertical Singlet Electronic Energies, Δ*E*, Oscillator Strengths, *f*, and Main Transition for BODIPY Molecules in Dichloromethane (*and Water*) Solvent[a]

	Δ*E* (eV, nm)	*f*	configuration	exptl λ_{abs} (nm)
1	2.372, 523	0.731	H → L, 70.7%	570
	(2.401, 516)	*(0.705)*	*(H → L, 70.7%)*	
2	2.273, 545	0.722	H → L, 70.7%	600
	(2.299, 539)	*(0.698)*	*(H→L, 70.7%)*	
3	2.250, 551	0.763	H → L, 70.7%	609
	(2.276, 545)	*(0.740)*	*(H → L, 70.7%)*	
4	2.193, 565	0.799	H → L, 70.7%	629
	(2.216, 560)	*(0.776)*	*(H → L, 70.7%)*	
5	2.398, 517	0.716	H → L, 70.6%	563
	(2.426, 511)	*(0.692)*	*(H → L, 70.6%)*	
6	2.268, 547	0.727	H → L, 70.6%	599
	(2.293, 541)	*(0.705)*	*(H → L, 70.6%)*	
7	2.202, 563	0.743	H → L, 70.6%	619
	(2.226, 557)	*(0.723)*	*(H → L, 70.6%)*	
8	2.288, 542	0.771	H → L, 70.7%	602
	(2.314, 536)	*(0.746)*	*(H → L, 70.7%)*	
9	1.868, 664	0.778	H → L, 70.7%	680
	(1.890, 656)	*(0.756)*	*(H → L, 70.7%)*	
10	1.892, 655	0.722	H → L, 70.6%	675
	(1.912, 648)	*(0.704)*	*(H → L, 70.6%)*	
11	2.182, 568	0.730	H → L, 70.5%	608
	(2.206, 562)	*(0.713)*	*(H → L, 70.5%)*	
12	1.947, 637	0.791	H → L, 70.7%	676
	(1.970, 629)	*(0.773)*	*(H → L, 70.7%)*	
13	2.253, 550	0.770	H → L, 70.4%	585
	(2.276, 545)	*(0.757)*	*(H → L, 70.3%)*	
14	2.142, 579	1.011	H → L, 70.3%	611
	(2.173, 571)	*(0.985)*	*(H → L, 70.3%)*	

[a]Experimental values are taken from ref 28.

From the reported data, a very satisfactory agreement between theory and experiment can be observed, the average error found in dichloromethane solvent being about 45 nm (about 0.1 eV). The maximum variation from experiment has been obtained for compound **2**, for which a difference of 64 nm has been computed. Furthermore, the variation of λ_{max} as a function of the rings substitution is excellently reproduced. All the Q transitions result to be HOMO → LUMO in nature (more than 70%) and with an oscillator strength higher than 0.7. Going from dichloromethane to water solvent, no significant changes in the wavelength absorbed have been observed (a difference of a few nm shifted in the blue region).

The excitation energy trend obtained for the studied compounds has been herein rationalized also considering the HOMO and LUMO energies (see Figure 1).

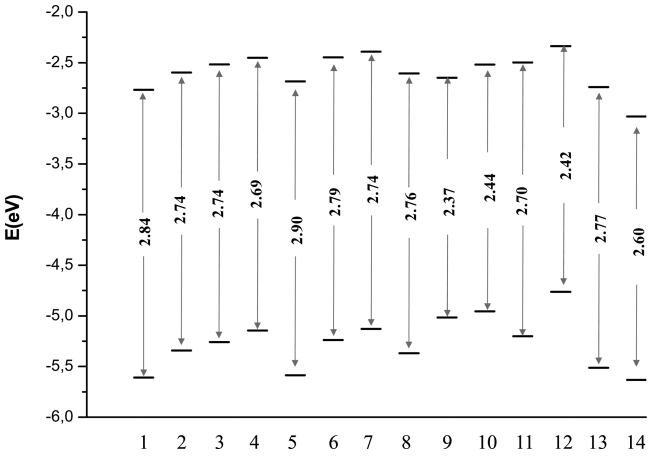

Figure 1. Energetic diagram for the highest occupied (HOMO) and lowest virtual unoccupied (LUMO) molecular orbitals of molecules **1**−**14**, obtained at M06/6-31+G* level of theory. The reported HOMO−LUMO energy gaps are in eV.

In the case of molecule **5**, the addition of a methyl group in the R position compared to molecule **1**, in which the R-R6 substituents are hydrogens, produces a shift of the absorption band at smaller wavelength, that is, from 570 to 563 nm. From Figure 1, it is possible to note that the addition of such electron donor species slightly increase the HOMO−LUMO (H-L) gap of 0.06 eV with respect to that found for the unsubstituted compound **1**.

In compounds **2**−**4** and **6**−**8**, it has been observed that the introduction of methyl groups on the rings B and C red shifts the Q absorption band as indicated by the reduction of their H-L gaps. As shown in Figure 1, this reduction is accomplished by a destabilization of both H and L energy levels with respect to that found in **1**.

Considering all the derivatives from **1** to **8**, the system with the absorption band at the highest wavelength results to be **4**, in which all the positions in rings C and D are occupied by $-CH_3$ and $-C_2H_5$ substituents. For that system, we find the smallest H-L gap (2.69 eV). The extension of the electron delocalization with the fusion of a benzene ring to the pyrrolic moiety (D) in **14** causes a further decrease of the H-L gap (2.60 eV) and, consequently, a red shift in the absorption Q-band (579 and 611 nm at theoretical and experimental levels, respectively).

Concerning the compounds **9**−**13**, it is worth to note that the species in which the Ar group is substituted in the R position (**11** and **13**) show absorption bands at the lowest wavelength and, consequently, the highest H-L gaps (2.70 and 2.77 eV). When R is linked to the position R_3 in ring C (species **9**, **10**, and **12**), the H-L energy gap decreases (see Figure 1) and the absorption is red-shifted up to 650 nm (see Table 3).

In order to have further insights on the increase or decrease of electron density upon electronic transition, the density difference between the first excited state and the ground state have been computed for the molecules with Ar groups **9**−**13** (Figure 2).

dx.doi.org/10.1021/ct500426h | J. Chem. Theory Comput. XXXX, XXX, XXX−XXX

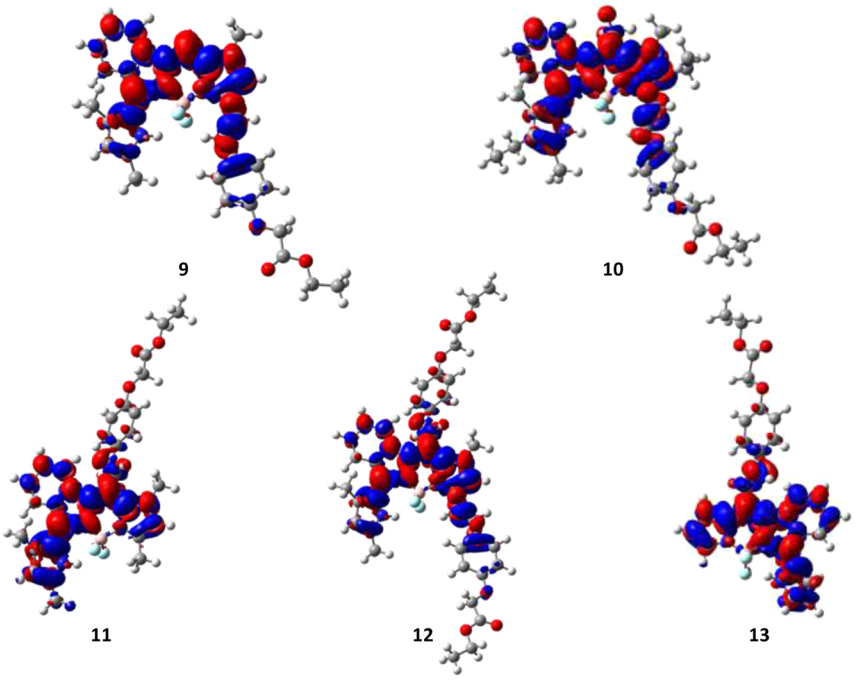

Figure 2. Computed density difference plots for **9**–**13**, with the first excited state considered (isodensity value of 5×10^{-4} a.u.); the red (blue) regions indicating increase (decrease) in the electronic density upon electronic transition.

Table 4. Vertical Singlet–Triplet Energy Gap in eV (ΔE_{S-T}) Computed in Water at M06/6-31+G* Level of Theory and Spin–Orbit Cartesian Matrix Elements between First Lowest Singlet and Triplet Excited States, Calculated at the B3LYP/6-31G(d)//M06

	ΔE_{S-T} (eV)	$\widehat{H_{SO}^{x}}$ (cm^{-1})	$\widehat{H_{SO}^{y}}$ (cm^{-1})	$\widehat{H_{SO}^{z}}$ (cm^{-1})	$\lvert\hat{H}_{SO}\rvert$ (cm^{-1})
1	1.35	−0.336	−0.740	−0.744	1.102
		(−0.380)[a]	(−0.836)[a]	(−0.689)[a]	(1.148)[a]
2	1.28	0.184	0.551	−0.358	0.682
3	1.28	−0.075	1.154	−0.566	1.287
4	1.24	−0.011	−0.191	−0.088	0.210
5	1.43	−0.057	−0.062	−0.061	0.104
6	1.35	0.035	0.461	−0.226	0.515
7	1.31	0.127	0.435	−0.151	0.478
8	1.27	−0.103	−0.435	−0.259	0.517
9	1.05	0.086	0.112	0.503	0.522
10	1.14	−0.020	−0.083	−0.046	0.097
11	1.31	0.066	0.173	0.553	0.583
12	1.16	0.105	0.007	0.312	0.329
13	1.37	−0.167	0.031	−0.334	0.375
14	1.25	1.137	0.520	0.331	1.293

[a]Breit–Pauli method.

The electron density difference maps allow to visualize the electronic rearrangement for a transition, with red regions denoting an accumulation of density and blue ones representing a depletion upon excitation. The phenyl ring of Ar group seems to be involved in the electronic rearrangement upon transition, only when it occupies the R3 position. Indeed, in the **9**, **10** and **12** density difference plots, a blue region can be detected consistent with the weak donor character of the phenyl moiety. Contrariwise, when it is in R position, no depletion zone can be observed. Such different involvement of Ar groups in the electron promotion process appears more evident in the density variation plot generated for compound **12**, in which the Ar group occupy both the positions (R and R3). The participation of the phenyl ring in the charge transfer observed in the case of **9**, **10** and **12** molecules, is accompanied by a shift of the absorption Q band toward higher wavelengths. From the computed density difference, it emerges that, in all studied systems, the transitions have quadrupolar nature with charge transfer depending on the substituent chemical nature and on the position. This behavior is similar to that revealed in a recent study on other borico dyes.[41]

The computed vertical energy gaps between singlet ground and low-lying triplet electronic states (ΔE_{S-T}) are reported in Table 4. Since we are checking the possibility that the considered compounds could be proposed as photosensitizers in PDT, which operate in a water-like environment (e.g.,

dx.doi.org/10.1021/ct500426h | J. Chem. Theory Comput. XXXX, XXX, XXX–XXX

physiological medium), ΔE_{S-T} have been computed in water solvent. All the compounds have ΔE_{S-T} gaps higher than that necessary to activate the oxygen molecule from its triplet ground to the singlet excited state (0.98 eV).[20]

The highest value is possessed by compound **5**, in which only a methyl group is present in position R as substituent. As already underlined, such a compound possesses also the highest H-L gap and, consequently, the highest excitation energy and the smallest wavelength.

Furthermore, we underline that the presence of the Ar group in position R3 (compounds **9**, **10**, **12**) contributes to sensibly reduce the gap (1.05, 1.14, and 1.16 eV, respectively).

A comparison between similar BF_2-chelated tetraarylazadipyrromethene dyes previously studied from a theoretical point of view[36] reveals that the presence of an isoindole group sensibly contributes to increase the value of this important PDT parameter.

3.3. Spin−Orbit Coupling Constants. As mentioned in the Introduction, the performance of a photosensitizer to act as a drug in PDT is strictly related to the singlet oxygen cytotoxic agent promotion. This production depend on the efficiency of the intersystem crossing (radiationless transition $S_1 \rightarrow T_1$ rate constants) that, in turn, depends on the amplitude of the spin−orbit coupling. This last term is proportional to the squared module of the spin−orbit Hamiltonian matrix element between the initial Ψ (S_1) and final Ψ (T_1) wave functions and can depend on different factors, such as the nature of the orbitals involved in the transition or the presence in the molecular system of a heavy atom. The spin−orbit matrix elements can be computed by using the more accurate Breit−Pauli method or the atomic mean field approximation.[55,56] The former is more rigorous but requires higher computational efforts. Although previous studies have demonstrated that the two procedures give almost the same values,[29,30,34] the spin−orbit matrix elements for compound **1** have been calculated by using both methodologies. As shown in Table 3, also in this case, the obtained values are very similar: the $|\hat{H}_{SO}|$ is 1.102 and 1.148 cm^{-1} at the atomic mean field approximation and the Breit−Pauli method, respectively. Because of this excellent agreement, the less demanding atomic mean field approximation has been used for all the other compounds. Compounds **1**, **3**, and **14** ($|\hat{H}_{SO}|$ = 1.1, 1.3, 13.3 cm^{-1}, respectively) have the highest SO coupling, whereas **5** has the lowest ($|\hat{H}_{SO}|$ = 0.1 cm^{-1}). It is difficult to rationalize these results, but in general, the key concept to understand the trend of the SO matrix elements lies in the nature of the MOs involved in the coupling mechanism (see Figure S1, Supporting Information, for ground state HOMO and LUMO orbital composition) arising from the one electron singlet and triplet transition (S_1 and T_1 in our case) states. In particular, the best orbital orientation for SO mixing is when the two p orbitals are at 90° with respect to one another since, in order to generate angular momentum, an orbital jump is required. Furthermore, a further complication occurs when the discoincident orbitals are the same orbitals, as for the $\langle S_1|H_{SO}|T_1\rangle$ values in our systems.

3.4. Photodynamic Therapy Properties. The drugs that are used in Type II PDT must efficiently generate the cytotoxic singlet oxygen ($^1O_2$) species throughout the following process:

$$PS(T_1) + {}^3O_2 \rightarrow PS(S_0) + {}^1O_2$$

This means that the S_1 energy of the photosensitizer (PS) can be transferred to the T_1 state via a radiationless intersystem spin-crossing (ISC) and, if the T_1 energy of the photosensitizer lies above the energy necessary to activate the ground state molecular oxygen (0.98 eV), the excited singlet molecular oxygen is generated. The efficiency of the ISC will depend on the amplitude of the spin−orbit matrix elements, as evident from the following relationship

$$K_{ISC} = \frac{4\pi^2}{h} |\langle \Psi_{S_1}|\hat{H}_{SO}|\Psi_{T_1}\rangle|^2 F_\nu \cdot \rho(E_f)$$

where the terms F_ν and ρ (E_f) are, respectively, the Franck−Condon factor and the density of vibrational states for the final state T_1.

Another condition to be realized for the therapy of solid tumors by PDT is the employment of light with an appropriate wavelength to penetrate into the tissues.

In particular, good PDT photosensitizers should have an absorption band that falls in the so-called photodynamic therapy window (500−900 nm). In Figure 3, we have collected

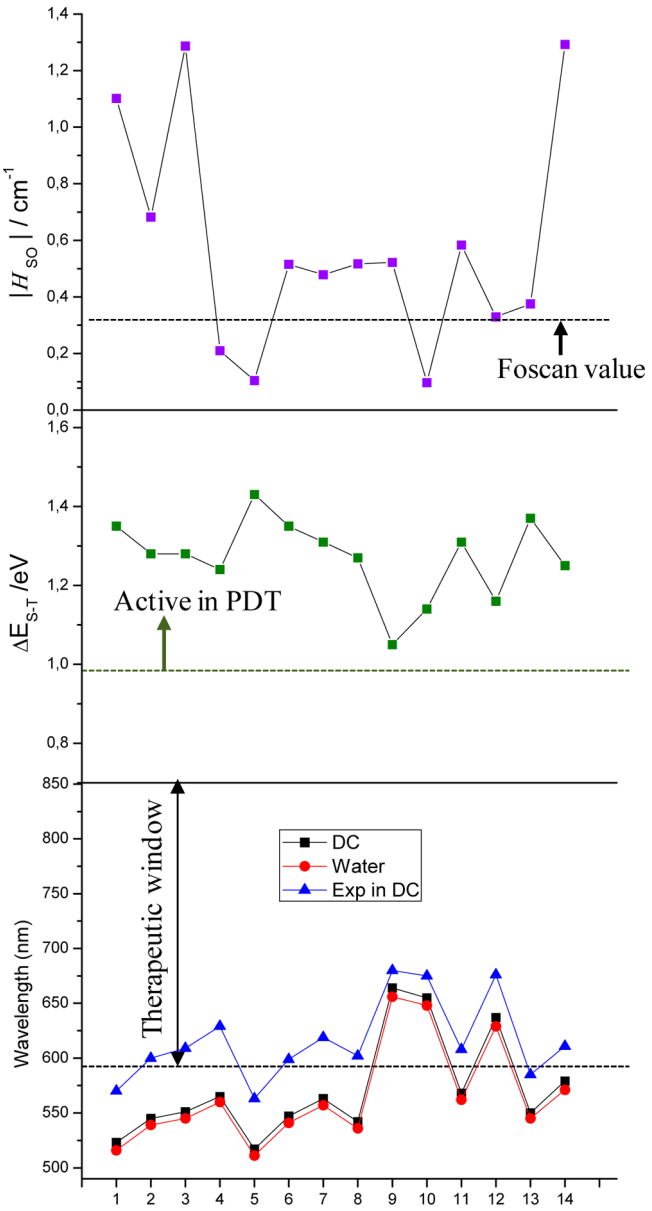

Figure 3. Plot of spin−orbit coupling constants ($|\hat{H}_{SO}|$), singlet−triplet energy gaps (ΔE_{S-T}), and Q-band absorption wavelengths values for the considered isoindole-BODIPY-like systems.

dx.doi.org/10.1021/ct500426h | J. Chem. Theory Comput. XXXX, XXX, XXX−XXX

the relevant PDT photophysical properties of the studied compounds in comparison with Foscan (5,10,15,20-tetrakis(*m*-hydroxyphenyl)chlorin), a photosensitizer approved and used for PDT treatment of a series of diseases, including head and neck cancer. From this figure, it is evident that only **1**, **5**, and **13** compounds have an absorption wavelength that lies below the therapeutic window. The systems that are able to better penetrate in the tissue are **9**, **10**, and **12** with absorption maxima of 680 (664), 675 (655), and 676 (637) nm, respectively, at experimental and theoretical (in parentheses) levels. The corresponding absorption values in Foscan are 650 nm (experiment) and 596 nm (theory).[29] Concerning the ΔE_{S-T} gap, all the considered compounds show values sufficient to excite the O_2 from its triplet ground state to singlet excited ones (0.98 eV). In particular, we underline the high values for the **1** (1.35 eV), **5** (1.43 eV), **11** (1.31 eV), and **13** (1.37 eV) systems. Comparing the spin−orbit coupling values, we note that, with the exception of **4**, **5**, and **10** systems, all the others have values higher than the Foscan counterpart. Therefore, the compounds with the highest ISC probability are **1**, **3**, and **14**.

4. CONCLUSIONS

In this paper, we have theoretically determined the photophysical properties of a series of recently synthesized isoindole-boron dipyrromethene derivatives. In particular, we have concentrated our attention on the absorption wavelengths, singlet−triplet energy gaps, and the spin−orbit matrix elements for the radiationless $S_1 \rightarrow T_1$ coupling because of their importance in photodynamic therapy. From our study, the following conclusions can be drawn:

- The M06 exchange-correlation functional gives absorption wavelengths closer to the experimental values with an error of less than 0.1 eV.
- Almost all the studied isoindole-BODIPY systems show Q-band peaks higher than 600 nm and in the range of the so-called therapeutic window.
- All the examined compounds show ΔE_{S-T} gaps able to generate the cytotoxic singlet molecular oxygen.
- The majority of the examined compounds possess spin−orbit matrix elements higher than those found for the reference Foscan molecule.

Linking together these three properties, we can indicate the compounds **2**, **3**, **14**, **6**−**9**, **11**, and **12** as photosensitizer candidates in type II photodynamic therapy. We hope that our work can stimulate future and desirable experimental studies and, in particular, biological tests.

■ ASSOCIATED CONTENT

Ⓢ Supporting Information

Cartesian coordinates of the investigated isoindole-BODIPY dyes and molecular orbital plots. This material is available free of charge via the Internet at http://pubs.acs.org.

■ AUTHOR INFORMATION

Corresponding Authors

*E-mail: malberto@unical.it (M.E.A.).
*E-mail: desimone@unical.it (B.C.D.S.).

Notes

The authors declare no competing financial interest.

■ ACKNOWLEDGMENTS

We thank the Università della Calabria for the financial support.

■ REFERENCES

(1) Loudet, A.; Burgess, K. *Chem. Rev.* **2007**, *107*, 4891.
(2) Ulrich, G.; Ziessel, R.; Harriman, A. *Angew. Chem., Int. Ed.* **2008**, *47*, 1184.
(3) Boens, N.; Leen, V.; Dehaen, W. *Chem. Soc. Rev.* **2012**, *41*, 1130.
(4) Rogers, M. A. T. *Nature* **1943**, *151*, 504.
(5) Tribs, A.; Kreuzer, F. U. *Justus Liebigs Ann. Chem.* **1986**, *718*, 208.
(6) Killoran, J.; Allen, L.; Gallagher, J. F.; Gallagher, W. M.; O'Shea, D. F. *Chem. Commun.* **2002**, 1862.
(7) Gorman, A.; Killoran, J.; O'Shea, C.; Kenna, T.; Gallagher, W. M.; O'Shea, F. D. *J. Am. Chem. Soc.* **2004**, *126*, 10619.
(8) Awuah, S. G.; You, Y. *RCS Adv.* **2012**, *2*, 11169.
(9) Kamkaew, A.; Lim, S. H.; Lee, H. B.; Kiew, L. V.; Chung, L. Y.; Burgess, K. *Chem. Soc. Rev.* **2013**, *42*, 77.
(10) Agostinis, P.; Berg, K.; Keith, A.; Cengel, M. D.; Foster, T. H.; Girotti, A. W.; Gollnick, S. O.; Hahn, S. M.; Hamblin, M. R.; Juzeniene, A.; Kessel, D.; Korbelik, M.; Moan, J.; Mroz, P.; Nowis, D.; Piette, J.; Wilson, B. C.; Golab, J. *Ca-Cancer J. Clin.* **2011**, *61*, 250.
(11) Dolmans, D. E.; Fukumura, D.; Jain, R. K. *Nat. Rev. Cancer* **2003**, *3*, 380.
(12) Dougherty, T. J.; Gomer, C. J.; Henderson, B. W.; Jori, G.; Kessel, D.; Korbelik, M.; Moan, J.; Peng, Q. *J. Natl. Cancer Inst.* **1998**, *90*, 889.
(13) MacCormack, M. A. *Semin. Cutaneous Med. Surg.* **2008**, *27*, 52.
(14) Dougherty, T. J. *J. Clin. Laser Med. Surg.* **2002**, *20*, 3.
(15) Juzeniene, A.; Peng, Q.; Moan, J. *Photochem. Photobiol. Sci.* **2007**, *6*, 1234.
(16) Babilas, P.; Schreml, S.; Landthaler, M.; Szeimies, R. M. *Photodermatol., Photoimmunol. Photomed.* **2010**, *26*, 118.
(17) Kossodo, S.; LaMuraglia, G. M. *Am. J. Cardiovasc. Drugs* **2001**, *1*, 15.
(18) Garrier, J.; Bezdetnaya, L.; Barlier, C.; Grafe, S.; Guillemin, F.; D'Hallewin, M. A. *Photodiagn. Photodyn. Ther.* **2011**, *8*, 321.
(19) Schweitzer, C.; Schmidt, R. *Chem. Rev.* **2003**, *103*, 1685.
(20) Herzberg, G. *In Spectra of Diatomic Molecules*, 2nd ed.; Van Nostrand Reinhold: New York, 1950; pp 344−346.
(21) Wu, L.; Burgess, K. *Chem. Commun.* **2008**, 4933.
(22) Banfi, S.; Caruso, E.; Caprioli, S.; Mazzagatti, L.; Canti, G.; Ravizza, R.; Gariboldi, M.; Monti, E. *Bioorg. Med. Chem.* **2004**, *12*, 4853.
(23) Hsi, R. A.; Kapatkin, A.; Strandberg, J.; Zhu, T.; Vulcan, T.; Solonenko, M.; Rodriguez, C.; Chang, J.; Saunders, M.; Mason, N.; Hahn, S. *Clin. Cancer Res.* **2001**, *7*, 651.
(24) O'Connor, A. E.; William, M.; Gallagher, W. M.; Byrne, A. T. *Photochem. Photobiol.* **2009**, *85*, 1053.
(25) Wainwright, M. *Chem. Soc. Rev.* **1996**, *25*, 351.
(26) New, O. M.; Dolphin, D. *Eur. J. Org. Chem.* **2009**, *16*, 2675.
(27) Ramaiah, D.; Eckert, I.; Arun, K. T.; Weidenfeller, L.; Epe, B. *Photochem. Photobiol.* **2002**, *76*, 672.
(28) Yu, C.; Xu, Y.; Jiao, L.; Zhou, J.; Wang, Z.; Hao, E. *Chem.—Eur. J.* **2012**, *18*, 6437.
(29) Alberto, M. E.; Marino, T.; Quartarolo, A. D.; Russo, N. *Phys. Chem. Chem. Phys.* **2013**, *15*, 16167.
(30) Alberto, M. E.; Iuga, C.; Quartarolo, A. D.; Russo, N. *J. Chem. Inf. Model.* **2013**, *53*, 2334.
(31) Mazzone, G.; Russo, N.; Sicilia, E. *Can. J. Chem.* **2013**, *91*, 902.
(32) Fortes Ramos Sousa, F.; Quartarolo, A. D.; Sicilia, E.; Russo, N. *J. Phys. Chem. B* **2012**, *116*, 10816.
(33) Quartarolo, A. D.; Russo, N. *J. Chem. Theory Comput.* **2011**, *7*, 1073.
(34) Quartarolo, A. D.; Chiodo, S. G.; Russo, N. *J. Chem. Theory Comput.* **2010**, *6*, 3176.
(35) Quartarolo, A. D.; Sicilia, E.; Russo, N. *J. Chem. Theory Comput.* **2009**, *5*, 1849.

(36) Quartarolo, A. D.; Russo, N.; Sicilia, E. *Chem.—Eur. J.* **2006**, *12*, 6797.
(37) Jacquemin, D.; Perpete, E. A.; Ciofini, I.; Adamo, C. *Acc. Chem. Res.* **2009**, *42*, 326.
(38) Eriksson, E. S. E.; Eriksson, L. A. *Phys. Chem. Chem. Phys.* **2011**, *13*, 7207.
(39) Jacquemin, D.; Perpete, E. A.; Scuseria, G. E.; Ciofini, I.; Adamo, C. *J. Chem. Theory Comput.* **2008**, *4*, 123.
(40) Adamo, C.; Jacquemin, D. *Chem. Soc. Rev.* **2013**, *42*, 845.
(41) Charaf-Eddin, A.; Le Guennic, B.; Jacquemin, D. *Theor. Chem. Acc.* **2014**, *133*, 1456.
(42) Frisch, M. J.; Trucks, G. W.; Schlegel, H. B.; Scuseria, G. E.; Robb, M. A.; Cheeseman, J. R.; Scalmani, G.; Barone, V.; Mennucci, B.; Petersson, G. A.; Nakatsuji, H.; Caricato, M.; Li, X.; Hratchian, H. P.; Izmaylov, A. F.; Bloino, J.; Zheng, G.; Sonnenberg, J. L.; Hada, M.; Ehara, M.; Toyota, K.; Fukuda, R.; Hasegawa, J.; Ishida, M.; Nakajima, T.; Honda, Y.; Kitao, O.; Nakai, H.; Vreven, T.; Montgomery, J. A., Jr.; Peralta, J. E.; Ogliaro, F.; Bearpark, M.; Heyd, J. J.; Brothers, E.; Kudin, K. N.; Staroverov, V. N.; Kobayashi, R.; Normand, J.; Raghavachari, K.; Rendell, A.; Burant, J. C.; Iyengar, S. S.; Tomasi, J.; Cossi, M.; Rega, N.; Millam, J. M.; Klene, M.; Knox, J. E.; Cross, J. B.; Bakken, V.; Adamo, C.; Jaramillo, J.; Gomperts, R.; Stratmann, R. E.; Yazyev, O.; Austin, A. J.; Cammi, R.; Pomelli, C.; Ochterski, J. W.; Martin, R. L.; Morokuma, K.; Zakrzewski, V. G.; Voth, G. A.; Salvador, P.; Dannenberg, J. J.; Dapprich, S.; Daniels, A. D.; Farkas, Ö.; Foresman, J. B.; Ortiz, J. V.; Cioslowski, J.; Fox, D. J. *Gaussian 09*, Revision A.2; Gaussian, Inc.: Wallingford, CT, 2009.
(43) Casida, M. E. In *Recent Developments and Applications in Density-Functional Theory*; Seminario, J. M., Ed.; Elsevier: Amsterdam, The Netherlands, 1996; pp 155−192.
(44) Zhao, Y.; Truhlar, D. G. *J. Theor. Chem. Acc.* **2008**, *120*, 215.
(45) (a) Chai, J.-D.; Head-Gordon, M. *Phys. Chem. Chem. Phys.* **2008**, *10*, 6615;(b) *J. Chem. Phys.* **2008**, *128*, 84106.
(46) Adamo, C.; Barone, V. *J. Chem. Phys.* **1999**, *110*, 6158.
(47) Adamo, C.; Barone, V. *J. Chem. Phys.* **1999**, *110*, 6158.
(48) Ernzerhof, M.; Scuseria, G. E. *J. Chem. Phys.* **1999**, *110*, 5029.
(49) Cossi, M.; Barone, V. *J. Chem. Phys.* **2000**, *112*, 2427.
(50) Tomasi, J.; Menucci, B.; Cammi, R. *Chem. Rev.* **2005**, *105*, 2999.
(51) *DALTON: A Molecular Electronic Structure Program*; 2011. http://daltonprogram.org/.
(52) (a) Becke, A. D. *Phys. Rev. A* **1988**, *38*, 3098;(b) *J. Chem. Phys.* **1993**, *98*, 5648.
(53) Lee, C.; Yang, W.; Parr, R. G. *Phys. Rev. B* **1988**, *37*, 785.
(54) Furche, F.; Ahlrichs, R. *J. Chem. Phys.* **2002**, *117*, 7433.
(55) Ågren, H.; Vahtras, O.; Knuts, S.; Jørgensen, P. *Chem. Phys.* **1994**, *181*, 291.
(56) Ruud, K.; Schimmelpfennig, B.; Ågren, H. *Chem. Phys. Lett.* **1999**, *27*, 215.